SCC OF ANNEALED AND COLD WORKED TITANIUM GRADE 7 AND ALLOY 22 IN 110 °C CONCENTRATED SALT ENVIRONMENTS

P.L. Andresen, P.W. Emigh, L.M. Young
GE Corp. Research & Development
One Research Circle Room 3A39
Schenectady, NY 12309

G.M. Gordon
Framatome Cogema Fuels
1211 Town Center Drive
Las Vegas, NV 89134

ABSTRACT

Stress corrosion crack growth studies have been performed on annealed and cold worked Titanium Grade 7 and Alloy 22 in 110 °C, aerated, concentrated, high pH salt environments characteristic of concentrated ground water. Following a very careful transition from fatigue precracking conditions to SCC conditions, the long term behavior under very stable conditions was monitored using reversing dc potential drop. Titanium Grade 7 exhibited continuous crack growth under both near-static and complete static loading conditions. Alloy 22 exhibited similar growth rates, but was less prone to maintain stable crack growth as conditions approached fully static loading.

Keywords: Stress corrosion cracking, Alloy 22, Titanium Grade 7, crack growth rate, concentrated groundwater, nuclear waste.

INTRODUCTION

This program is designed to characterize the stress corrosion crack growth rate response of waste canister structural materials for the Yucca Mountain Project. The waste package is one of the few elements of the project that can be engineered, and the ability to provide very long waste package lifetimes that can be predicted with confidence is a central factor in the release rate of radionucleides from the mountain.

General corrosion, localized corrosion and stress corrosion cracking represent the most likely degradation modes for the waste package structural materials. One key to demonstrating and predicting the

long waste package lifetimes lies in characterizing the local environment that forms on the waste package. This is particularly important for temperatures above ≈ 75 °C, where the heat flux through the waste package is higher, the environments are more concentrated, and the material susceptibility to corrosion degradation is highest. The waste package is always hotter than its surrounding environment, probably by several degrees at ≥ 70 °C. Since it is reasonable to assume that water reaches the tunnel walls, and that the higher surface area of the tunnel walls controls the air temperature and maintains relative humidity at 100%, any liquid that forms on the waste package must concentrate sufficiently for the temperature differential (e.g., 2 – 5 °C) of the waste package. Whether from dripping / splashing ground water, contaminants from handling, or rock dust and atmospheric aerosols (during construction / ventilation), it is hard to preclude the prospect of aqueous films forming on the waste package. The most likely scenario relates for ground water type compositions that concentrate (or hydrate) on the waste package to form a solution concentration on the waste package surface of at least several molar. The concentration of any aqueous phase will decrease with time / temperature, although even after >>10,000 years, a waste package temperature of 40 or 50 °C is expected, and this brings with it an aqueous phase of about one molar solution. As the mobile water in Yucca Mountain concentrates, its mixed ion character remains intact, and its pH rises to at least 9 or 10. This is a much more benign environment than a hot, concentrated, acidified chloride that was envisioned early in the Project.

Other programs are addressing the general and localized corrosion in these and related environments. The objective of this program is to measure the stress corrosion crack growth rates under conditions that are both relevant and likely to promote stress corrosion cracking, i.e., fairly high concentrations at fairly high temperature.

EXPERIMENTAL PROCEDURES

This program utilized fracture mechanics, crack growth rate (1-inch compact type (1TCT) or, for cold worked materials, 0.5T CT specimens) specimens of Alloy 22 and Titanium Grade 7; subsequent tests may evaluate Titanium Grade 16 and perhaps Type 316 NG stainless steel. Materials were supplied in specimen form by the Project in the solution annealed condition. All materials were provided by TRW and have been tested in the as-received and in the 20% cold worked condition. The 20% cold work was performed by GE CRD by cross-rolling at room temperature by about 10% in each direction. Because the resulting plate was thinner, only 0.5-inch (0.5TCT) specimens could be produced, but because of the higher yield strength of the cold worked material, they were fully linear elastic at 30 MPa$\sqrt{m}$ as specified by criteria in ASTM E399 and E647. Crack length was monitored in-situ using a reversing dc potential drop technique [1].

Most specimens were fatigue pre-cracked in air (some were done in the environment), with the ending phase at the K_{max} used for SCC testing (typically 30 MPa$\sqrt{m}$) at a load ratio R of 0.7. Each specimen was assembled in an autoclave and tested in the specified chemistry at the corrosion potential. Solution annealed (as-received) and 20% cold worked Alloy 22 and Titanium Grade 7 were tested at 30 MPa$\sqrt{m}$, and one 1TCT specimen of as-received Alloy 22 is being tested at 45 MPa$\sqrt{m}$. A complete transition from fatigue pre-cracking conditions to stress corrosion cracking conditions was made by continuing the cycling (generally at a load ratio R = 0.7) at a very low frequency (0.001 Hz) and eventually to increasingly long hold times (e.g., ≥ 9,000 s) at K_{max}. "Gentle" unloading cycles are used to help ensure that optimal results are obtained [2-3].

Careful selection of the environments to be evaluated is crucial, because the stress corrosion cracking results may be highly biased if, e.g., pitting or crevice corrosion occurs. These initial tests were performed in

water that simulates the concentrated environment that must form on a hot waste package (net heat flux from the waste package means that the local environment is always concentrated, if not saturated). The mix of chemicals used for the test chemistry is shown below:

10.6 g Na_2CO_3 (anhydrous)	9.7 g KCl
8.8 g NaCl	0.2 g NaF
13.6 g $NaNO_3$	1.4 g Na_2SO_4 (anhydrous)
4.1 g $Na_2SiO_3*9H_2O$	55.3 g H_2O

In the first test (c143), the chemicals were mixed with water that had been heated to the boiling point in the four liter autoclave. However, the target composition did not fully dissolve in water, leaving some solids in the autoclave. For the subsequent tests (c144, c148, c152, and c153), the chemicals were mixed with water maintained at the boiling point in a Teflon beaker for ≈ 60 minutes, then the solution (not the solids) was poured into the autoclave. Initial testing was performed in either a Hastelloy C-276 autoclave body or a commercial purity titanium autoclave; however, a third system was started to accommodate test c153, and only a stainless steel body was available. However, some stainless steel has been present in all test autoclaves, and there has been no evidence of its corrosion. Solution was periodically sampled from the autoclaves during the test, as presented in the Results and Discussion section.

Control of dissolved oxygen is important, and near the boiling point of a solution the dissolved gas concentration varies markedly with temperature. To avoid extreme variations (and very low average dissolved oxygen concentrations), slowly flowing laboratory air was kept pressurized at 5 psig throughout the test. The exact concentration of dissolved oxygen can only be estimated. While the solubility of dissolved oxygen at 110 °C is well known in pure water [4], the "salting out" effect of this particular chemistry and at 110 °C is not precisely known. Assuming that the "salting out" effect decreases the dissolved oxygen concentration by 2X compared to pure water (the solubility of O_2 in 110 °C water is 25.6 ppm per atmosphere partial pressure of O_2), the dissolved oxygen level should be about 0.91 ppm (25.6 ppm/atm x 20.9% O_2 in air x 5 psi / 14.7 psi/atm divided by 2 for the "salting out" effect).

To prevent evaporative loss of water, a four foot long tube-in-tube heat exchanger was used, with cooling water on the outside. A back pressure regulator at the outlet of the autoclave gas space was used to maintain the desired (5 psi) system pressure. The water level in the autoclave was checked periodically by checking for continuity between the autoclave and an insulated stainless steel feed-through bar, and by occasional visual inspection which entailed a brief depressurization of the system. No water addition was needed.

Measurements of corrosion potential were complicated by the operation of the system near the boiling point. Thus, the solution in traditional internal or external Ag/AgCl electrodes containing 0.01 or 0.1 N KCl would boil at 110 °C, and zirconia membrane reference electrodes have very high resistivity at <150 °C. Thus, a modified external Ag/AgCl reference electrode was used which employed a 4 N KCl solution. There are no data for these electrodes at high chloride concentrations, but the conversion to V_{she} was estimated to be +0.110 V_{she} by evaluating literature data over a range of chloride concentrations and temperatures and extrapolating to 4 N. Thus, 0.110 V_{she} is added to the measured values to produce V_{she}.

RESULTS AND DISCUSSION

Specimen c143 of As-Received Titanium Grade 7

Following air fatigue precracking and assembly into the autoclave, the specimen was held at 11 MPa$\sqrt{m}$ while the temperature controller was tuned to provide good stability vs. time and adjustments were made to the air pressurization system (bubbling of laboratory air through the autoclave solution was initially attempted, but the tube used for bubbling was repeatedly sealed off by encrustations of salt).

An overview of the stress corrosion test is shown in Figure 1. As shown in Figures 1 and 2, at 277 hours the specimen was loaded to 30 MPa$\sqrt{m}$ and a very low frequency cycle was imposed at R = 0.7 and 0.001 Hz. Following an initial period of high growth rate, the growth rate became quite well behaved at $\approx 8 \times 10^{-8}$ mm/s (Figure 2). At 1555 hours into the test, the loading was modified by introducing a 1,000 s hold time at K_{max} (making the duration of the hold time and the full cycle the same). This had little effect on crack growth rate, although the crack growth rate did slow down very slightly. Figure 2 (and the other figures that detail specific test segments) show the linear regression fits over the duration of the test segment graphed, along with the calculations for the best fit slope (growth rate), the slopes corresponding to the upper and lower 95% confidence level, and the correlation coefficient (R^2). The high correlation coefficient (1.0 represents a perfect correlation) and the very close agreement of the upper and lower 95% confidence slopes provide a high level of confidence in the quality of the observations.

At 2154 hours, a longer hold time (9,000 s) at K_{max} was initiated (Figures 1 and 3). This produced a decrease in crack growth rate of about 2X. The subsequent response was quite well behaved (Figure 3), although some tendency for the crack growth rate to decrease vs. time is evident. Nonetheless, when the entire data set shown in Figure 3 is evaluated, a good fit and high correlation coefficient are obtained, and the closeness of the upper and lower 95% confidence slopes strongly support the best fit crack growth rate of 4.0×10^{-8} mm/s.

At 2848 hours, a yet longer hold time (85,400 s) was introduced, yielding one unloading cycle per day (Figures 1 and 4). Again, a relatively crisp and well-behaved response was observed, with a best fit crack growth rate of 1.6×10^{-8} mm/s. At 3713 hours, the specimen was unloaded (but not cooled down) because of concern for power outages as the threshold into the year 2000 was crossed. On re-loading, a small, short-term transient was observed (Figure 1), which is not unusual given the deep loading cycle. The linear regression calculation for this transient period yields a growth rate of 1.6×10^{-8} mm/s, which is a reasonable representation of the static load behavior of an actively growing stress corrosion crack. This is borne out in the change to static load at 4073 hours (Figure 5) – during the nearly 2000 hours period of testing at static load, the growth rate was maintained very stable at 1.25×10^{-8} mm/s.

The distinction "actively growing" is crucial, because round robins [2,3] and other studies [5,6] have shown that there are many cases where cracks don't grow or temporarily cease growing that are "anomalous" – i.e., in many other cases under identical conditions, well-behaved, long-term crack growth is obtained. An extensive evaluation of crack growth data in nickel base alloys by a group of international experts [7] concluded that among the many experimental flaws in the available crack growth data, the failure to make a complete transition from fatigue precracking (which is transgranular and has different plastic zone characteristics than a stress corrosion crack) to an SCC crack is crucial, as is the use of at least occasional partial unloading to

maintain an active crack. A more detailed discussion of the origins and implications of this phenomenon has been made [8], which hypothesized that the large differences in observed "K_{Iscc}" among different laboratories and investigators is associated with both experimental problems and the inherent probabilistic nature of both SCC initiation and growth. Since few specimens / sites / microstructures can be evaluated in the lab (compared to the available opportunities in actual structures), it is crucial to quantify dependencies and overall susceptibility by maintaining an active crack, or else the vast noise in the data overwhelms the dependencies [2,3,6-8].

However, it is equally important to recognize that "active" SCC is not necessarily easy to maintain, and there is strong experimental evidence to suggest that the probability of maintaining "active" SCC (which is much higher than the probability of re-initiating SCC for a crack that has stopped) is related to the crack growth rate (fast cracks are much more likely to sustain their advance vs. time) and factors such as the creep rate, yield strength, etc. Compared to typical light water reactor operating temperatures of 274 to 340 °C (where extensive studies have been performed), the probability of sustaining SCC is significantly lower at ≤ 110 °C at more realistic stress intensity factors of <10 MPa√m (i.e., associated with the development of readily detectable cracks of > 10 – 15% of through-wall depth).

Another very important factor is the incidence of "transients" such as start up and shutdown, vibrations, changes in plant output, etc. that (like partial unloading) can induce crack re-initiation. In this regard, there has undoubtedly never been a human design that is expected to operate under more fully static conditions than the proposed Yucca Mountain repository, because (barring the occurrence of exceedingly unlikely and rare incidents, such as earthquakes) the system will change (cool) only in a *very slowly*, well controlled fashion involving thermal changes of perhaps < 1 °C per century once the waste package cools sufficiently to have an aqueous environment (e.g., <120 °C). This should provide a remarkably low probability of stress corrosion cracking, especially given the low growth rates that are already measured, which will be dramatically lower still at stress intensities relevant to crack development (e.g., << 10 MPa√m).

The test ended at 6060 hours, and the CT specimen was removed and broken apart by fatigue cracking in air. Optical evaluation of the fracture surface showed the dc potential drop readings to be in good agreement with the actual crack length. The average crack depth was 0.136-inch, with a minimum of 0.122-inch and a maximum of 0.159-inch. Dc potential drop showed growth of 0.138-inch, which represents less than 2% error, typical of many other tests performed in this laboratory. Post-test correction of crack growth rates is not merited. Scanning electron fractographs are shown in Figure 6.

Specimen c144 of As-Received Alloy 22

Following air fatigue precracking and assembly into the autoclave, the specimen was left unloaded while adjustments were made to the temperature controller. At 247 hours, the specimen was loaded to 11 MPa√m to equilibrate the dc potential drop system at the 110 °C test temperature. At 272 hours, the specimen was loaded to 30 MPa√m and a very low frequency cycle was imposed at R = 0.7 and 0.001 Hz (Figure 7).

Because there was little initial evidence of crack advance, at 345 hours the load ratio R was lowered to 0.5, at which point crack advance commenced, although at a relatively low growth rate of ≈ 2.5 x 10^{-8} mm/s (Figure 7). At ≈ 600 hours, there is a dip in the crack length vs. time signal that cannot be explained based on any change in the test conditions. The noise in the crack length vs. time signal was of lower periodicity (about 24 hours, perhaps from slightly greater fluctuations in room temperature) than for specimen c143. The

subsequent response was well-behaved, as shown in Figure 8. At 1184 hours the loading was changed to R = 0.6, 0.001 Hz; this initially produced little discernible change in the growth rate. Over the time interval shown (including some data at R = 0.6), the linear regression fit was 2.1 x 10^{-8} mm/s. Additionally, detailed calculations are shown for the best fit growth rate, the growth rates corresponding to the upper and lower 95% confidence levels, and the correlation coefficient (R^2). The high correlation coefficient and the close agreement of the upper and lower 95% confidence values provide a high level of confidence in the quality of the observations.

About 100 hours after making the change to R = 0.6, the crack growth rate apparently stopped (Figure 7). Because of this, the loading frequency was increased from 0.001 to 0.003 Hz at 1801 hours. This was sufficient to re-activate the crack (Figures 7 and 9) and produce well-behaved crack growth response for the subsequent 300+ hours. The best fit growth rate was 3.3 x 10^{-8} mm/s, with a very high correlation coefficient (R^2) of 0.988. Note that despite the increase in frequency by 3X, the growth rate only increased by about 60%, indicating a very strong environmental component of crack advance (if the crack were advancing by inert fatigue, its rate would be linear with frequency).

At 2137 hours, the frequency was returned to 0.001 Hz, and now the crack growth rate was sustained (Figures 7 and 10). At 2481 hours, the load ratio was increased to R = 0.65, and again the growth rate was sustained. Finally, at 3345 hours the specimen was unloaded (but not cooled down) out of concern for power outages as we entered the year 2000. However, no problems were encountered and, on re-loading, the crack growth rate has been identical to the prior period.

At 3705 hours, the cycling was made more gentle by changing to R=0.7, 0.001 Hz, and the crack growth rate was essentially unchanged (Figure 11). At 4405 hours a 3,000 s hold time was introduced, and cracking appeared to cease. On removing the hold time at 5125 hours, the crack re-initiated, although at a slightly lower rate than was observed earlier under identical loading conditions.

The greater tendency for cracking to slow or cease in Alloy 22 compared to Ti Grade 7 is consistent with the lower growth rates observed for Alloy 22. This is consistent among a range of materials that show that the propensity for "active cracking" to cease increases as the growth rate decreases. Estimates of the "active" growth rate under static conditions can be made from experience and from comparison with the data from specimen c143. Using a factor of 4 as a reasonable estimate for the enhancement associated with periodic unloading, the expected / estimated growth rate for Alloy 22 under static loading conditions might be between 1 – 2 x 10^{-9} mm/s, a low number indeed, and more difficult still to measure than the rates observed on specimen c143. Indeed, in few if any instances have measurements at these rates ever been made.

At 507 h into the test, the autoclave solution was sampled and then submitted to the Materials Characterization Laboratory at GE CRD. The results are shown below, and differ somewhat from the analysis of the solution used in test c143, perhaps because the undissolved solids were not left in the autoclave of this test. As with specimen c143, the sample liquid was stored, and then recently used to evaluate the room temperature and 100 °C pH of the test solution. After calibration and checks in two buffered solutions, the pH was measured at room temperature to be 13.42. The vial containing the relatively small volume (about 25 cc) of solution was then heated in a beaker of boiling water, and the pH at about 100 °C was found to be about 12.6. Note that the boiling point of this liquid is above 110 °C, so heating to 100 °C did not produce boiling

(or even consequential evaporation during the short measurement). While this is not completely representative of the autoclave test solution, which is at 110 °C, the difference should be very small indeed.

The test ended at 5698 hours, and CT specimen was removed and broken apart by fatigue cracking in air. Optical evaluation of the fracture surface showed the dc potential drop readings to be in good agreement with the actual crack length. The average crack depth is 0.120-inch, with a minimum of 0.104-inch and a maximum of 0.128-inch. Dc potential drop showed growth of 0.108-inch, which represents only about 10% error, typical of many other tests performed in this laboratory. Post-test correction of crack growth rates is not merited, because discrepancies almost are always associated with unevenness in the crack front and the evolution of the unevenness with time is not known. Scanning electron microscopic examination of the fracture surface shows a purely transgranular crack morphology (Figure 12).

Specimen c148 of 20% Cold Worked Titanium Grade 7

After air fatigue precracking and assembly into the autoclave, the specimen was loaded to K_{max} = 30 MPa$\sqrt{m}$ under a very low frequency loading cycle at R = 0.7 and 0.001 Hz, and a stable crack growth rate of 5 x 10^{-8} mm/s was observed (Figure 13). At 541 hours, a 1,000 s hold time at K_{max} was introduced, and the growth rate slowed by about 2X to 2.2 x 10^{-8} mm/s. The hold time was increased to 3,000 s at 993 hours, and the growth rate again slowed to about 1.5 x 10^{-8} mm/s. At 1298 hours, the hold time was extended to 9,000 s, and very little change in crack growth rate was observed. Unfortunately, a very slow leak developed along the Teflon sheathed Pt wires used for the dc potential drop measurements, and its cumulative effect was not recognized. Over a several week period the crack length measurements showed an increase but then became noisy, and an evaluation of the situation led to the conclusion that the liquid level had dropped below the CT specimen. The system was unloaded, cooled, dis-assembled, and cleaned. The slow leak was repaired and new solution was put into the system. On re-heating and re-loading, the crack length returned to the expected level.

Since the crack growth rate had slowed to ≈1 x 10^{-9} mm/s, at 2959 hours more aggressive cycling was re-introduced, and this caused an increase to 5.5 x 10^{-8} mm/s (Figure 14), similar to what had been observed earlier under the same loading conditions (Figure 13). After what may seem like a long time, but involved only about 0.2 mm of crack advance, the conditions were changed at 4270 hours to include a 1,000 s hold at K_{max} (Figure 14). The growth rate changed crisply to 3.4 x 10^{-8} mm/s. At about 4800 hours, the hold time was again increased to 3,000 s.

Corrosion potential measurements of the CT specimen vs. a Pt electrode and a 4N KCl external Ag/AgCl reference electrode were made continuously (Figure 15). Initially, as also observed in tests c143 and c144, the corrosion potentials of the CT specimen and Pt electrode were similar, but careful impedance checks of the reference electrode revealed some concerns for the formation of gas bubbles in the electrode. Because at 110 °C the autoclave solution is above the boiling point of pure water, a 4N KCl electrolyte was used in the Ag/AgCl reference electrodes (coupled with the 5 psi overpressure, no boiling should occur), although this is not a guarantee that gas bubbles will not form. To evaluate the concern, the reference electrode was rebuilt, and a fiber wick was introduced so that ionic continuity could be maintained even if some gas bubbles formed, and different potentials were indeed measured. However, the reference electrode still has an ionic junction through which dilution and contamination of its internal electrolyte can occur, either of which will cause its

reference potential to shift, as was also noted as time progressed. It is believed that the potential values measured shortly after rebuilding the reference electrode are reasonably accurate.

Because long term drift in reference electrodes with ion junctions is inevitable, the "raw" potential of the CT specimen vs. the Pt electrode was also measured. Since Pt should not react or undergo surface changes, its potential should be stable with time. In turn, this can show whether the corrosion potential of the CT specimen is stable. The response (Figure 15) showed little change in the corrosion potential of the CT specimen (vs. the Pt electrode), but considerable drift did occur in the Ag/AgCl reference electrode. The higher potential of Pt (evident from the negative potential of the CT specimen vs. the Pt electrode) is consistent with many other measurements in 100 – 300 °C solutions. These observations clearly indicate that the reference electrode used prior to rebuilding did develop impedance problems from gas bubbles (also evident from tests c152 and c153) but that, even after rebuilding, the reference electrode is subject to drift as its internal electrolyte changes composition.

The corrosion potentials observed in this study for Alloy 22 (about 0 to 100 mV_{she}) are similar to those reported by Farmer et al. [9,10] in polarization scans of Alloy 22 in air saturated (no CO_2), carbonate and silicate free, modified (pH = 13 by adding NaOH) basic saturated water (BSW-13) at 110 °C [Figure 5 [9]]. For Alloy 22 thermally aged at 700 °C for 10 hours, he observed a corrosion potential of about –0.227 V, and his reported conversion to V_{she} at 95 °C of 0.199 V (Table JF8 in Ref. [10]) translates to a corrosion potential of about –0.03 V_{she}. Possible differences in experiments (e.g., these SCC measurements were performed with 5 psi of air over-pressure) and differences in solution composition, metallurgical condition (no SCC studies have yet been performed for aged Alloy 22) can easily account for small differences in corrosion potential.

While the measurement of thermodynamic (i.e., V_{she}) corrosion potentials has proven difficult under these conditions, we believe that the initial measurements after rebuilding the Ag/AgCl reference electrode are reasonably accurate. More important, the change in the potential of the titanium or Alloy 22 materials vs. time seems to be very limited, and indeed the data uniformly shows a decrease in the potential of titanium or Alloy 22 vs. the Pt electrode. The Pt electrode should be a stable, reliable indicator, because the test conditions (temperature, solution pH at temperature, and dissolved oxygen concentration) should change very little during the test.

Additionally, there is no sensible, foreseeable mechanism for the corrosion potential of Alloy 22 or titanium to continue to rise indefinitely. It is not impossible to imagine that their potential might rise slightly following initial exposure, but under these conditions their passive films are so protective and stable that contributions from metal corrosion is infinitesimally small, and the redox reactions from the species in solution should be stable. This should also apply to the waste packages, although some increase in dissolved oxygen is expected as the solution on the waste package cools from its saturated boiling point by 10 – 20 °C. After that, the solubility of oxygen in water changes much less with temperature. This response is different than that in high temperature water, where there is a known tendency for the corrosion potential of stainless steel to rise following initial exposure to 288 °C water (even in that case, the potential stabilizes). In 288 °C water stainless steel has a moderate corrosion rate (especially after initial exposure), and its corrosion reaction can play a moderate role in determining the corrosion potential in pure water.

Specimen c152 of As-Received Alloy 22

Following air fatigue precracking and assembly into the autoclave, the specimen was loaded to K_{max} = 45 MPa$\sqrt{m}$ and a low frequency cycle was imposed at R = 0.7 and 0.01 Hz, and a stable crack growth rate of 2.3 x 10^{-7} mm/s (Figure 16). At 100 hours, the frequency was reduced to 0.001 Hz, and again a stable growth rate was observed, at 2.3 x 10^{-8} mm/s. At 645 hours a 3,000 s hold time at K_{max} was introduced, although because the growth rate seemed to be slowing down too much, it was shifted to 1,000 s hold at 809 hours, where a growth rate of ≈ 1.5 x 10^{-8} mm/s was observed. At 1103 hours, the hold time was returned to 3,000 s, and the crack growth rate slowed to ≈ 7 x 10^{-9} mm/s (Figures 16 and 17). At 1523 hours, there was a small temperature excursion, which may have slowed the crack growth rate slightly (Figure 17). At 1978 hours, the hold time at K_{max} was changed to 9,000 s, which slowed the growth rate to ≈ 1.3 x 10^{-9} mm/m. The growth rate slowly increased vs. time to ≈ 2.1 x 10^{-9} mm/s (Figure 18). At 3800 hours, the hold time is again increased to 85,400 s.

Corrosion potential measurements of the CT specimen vs. the Pt electrode and the 4N KCl external Ag/AgCl reference electrode were made continuously (Figure 19). Discussion of the reference electrode measurements was presented for test c148.

Specimen c153 of 20% Cold Worked Alloy 22

Following air fatigue precracking and assembly into the autoclave, the specimen was loaded to K_{max} = 30 MPa$\sqrt{m}$ and a very low frequency cycle was imposed at R = 0.7 and 0.003 Hz, and a stable crack growth rate of 1.7 x 10^{-8} mm/s was observed (Figure 20). At 721 hours, the frequency was reduced to 0.001 Hz, and the growth rate slowed to 5 x 10^{-9} mm/s. Given the low growth rates, the time-based behavior is very stable. However, it takes longer to accommodate a given amount of crack advance, which is usually necessary to promote stable crack growth as static load conditions are approached.

At ≈ 1200 hours there was an error in the load controller so that it stopped cycling. When this was resolved, the crack growth rate was essentially unchanged (Figure 21). At 1892 hours, a 1,000 s hold time at K_{max} was introduced, and the growth rate slowed immediately to 2.6 x 10^{-9} mm/s. At 3202 hours, the loading was changed to constant load, and after a brief transient at a higher rate, a very low growth rate of 5 x 10^{-10} mm/s was observed (Figures 21 and 22). This is a very low crack growth rate, but it clearly suggests that crack advance under static load conditions can be achieved in Alloy 22, as was expected from the data with periodic unloading.

Corrosion potential measurements of the CT specimen vs. a Pt electrode and the 4N KCl external Ag/AgCl reference electrode were made continuously (Figure 23). Discussion of the reference electrode measurements was presented in the section on specimen c148.

Preliminary SCC Growth Rate Predictions

Initial efforts to extend SCC prediction algorithms developed by Ford and Andresen [11,12] for stainless steels and nickel alloys in 288 °C pure water environments to these materials and environments are promising. While the temperature is much lower and the solutions are not similar to "pure water", the materials are highly corrosion resistant in this environment and are therefore expected to have rapid repassivation rates. In the slip dissolution model of environment advance, this corresponds to a high "n" value, e.g., n > 0.75. Figure 25 shows curves for n = 0.8 and 1.0, which provide reasonable agreement with the observed SCC

rates. More data are needed to evaluate a broader range of stress intensities, material conditions, and solution compositions.

CONCLUSIONS

Stable, long-term environmentally-assisted crack growth rates were measured on Alloy 22 and Titanium Grade 7 for all metallurgical conditions evaluated (annealed and 20% cold worked). Such results require that very careful attention to testing detail and protocol is employed. SCC under fully static load / stress intensity conditions was obtained at growth rates that could be measured with confidence (1.25×10^{-8} mm/s) on Titanium Grade 7, and at very low rates that are measurable only with difficulty (5×10^{-10} mm/s) on 20% cold worked Alloy 22. Preliminary predictions based on the slip dissolution model of crack advance provide reasonable agreement with observation.

Simpler tests, such as slow strain rate tests, do not have the sensitivity to detect very small levels of susceptibility to SCC as were measured in these studies. It should be noted that the environment is not aggressive to these two materials, with no evidence whatsoever of localized attack, even in creviced areas. Indeed, only very limited signs of attack have been observed on type 304 or 316 stainless steel system parts exposed in these environments during long term testing. In turn, the very low levels of SCC susceptibility will translate into very high resistance to SCC in long term, constant load tests on smooth specimens, which are now being undertaken. Current waste package design includes solution annealing of all welds but the final closure weld, which will be stress mitigated to reduce tensile stresses and/or make them compressive through as much as 6 – 9 mm of wall thickness.

REFERENCES

1. P.L. Andresen and C.L. Briant, "Environmentally Assisted Cracking of Types 304L/316L/316NG Stainless Steel in 288 °C Water," Corrosion, pp. 448-463, 1989.
2. P.L. Andresen, "IGSCC Crack Propagation Rate Measurement in BWR Environments: Executive Summary of a Round Robin Study", Report 98:27, ISSN 1104-1374, ISRN SKI-R-98/27-SE, SKI, 1999.
3. P.L. Andresen, K. Gott and J.L. Nelson, "Stress Corrosion Cracking of Sensitized Type 304 Stainless Steel in 288 °C Water: A Five Laboratory Round Robin", Proc. Ninth Int. Symp. on Environmental Degradation of Materials in Nuclear Power Systems - Water Reactors, AIME, 1999.
4. D.M. Himmelblau, J Chem Eng Data 5, 10, 1960.
5. P.L. Andresen, "Effects of Testing Characteristics on Observed SCC Behavior in BWRs", Paper #98137, Corrosion/98, NACE, 1998.
6. P.L. Andresen, "SCC Testing and Data Quality Consideration", 9th Int. Symp. on Environmental Degradation of Materials in Nuclear Power Systems - Water Reactors, AIME, 1999.
7. Unpublished results from P.L. Andresen and other in an EPRI sponsored, international experts "PEER" group which evaluated crack growth data for Alloy 600 and Alloy 182 weld metal, 1999.
8. P.L. Andresen, "Probabilistic Interpretation of SCC Initiation & Growth", Paper #99446, Corrosion/98, 1999. See also P.L. Andresen et al., "Immunity, Thresholds, and Other SCC Fiction", Proc. Staehle Symp. on Chemistry and Electrochemistryof Corrosion and SCC, TMS, Feb. 2001.
9. J. Farmer et al., "General and Localized Corrosion of Outer Barrier of High Level Waste Container in Yucca Mountain", ASME PVP Conference, Seattle, July 2000.
10. J. Farmer, "Waste Package Degradation Expert Elicitation Project", Rev. 1, Prepared by Geomatrix Consultants and TRW, June 1998.
11. P.L. Andresen and F.P. Ford, "Life Prediction by Mechanistic Modelling and System Monitoring of Environmental Cracking of Fe and Ni Alloys in Aqueous Systems", Matls Sci & Eng, A103, 167, 1988.

12. F.P. Ford and P.L. Andresen, "Corrosion in Nuclear Systems: Environmentally Assisted Cracking in Light Water Reactors", *Corrosion Mechanisms*, Ed. P. Marcus and J. Ouder, M. Dekker, 501, 1994.

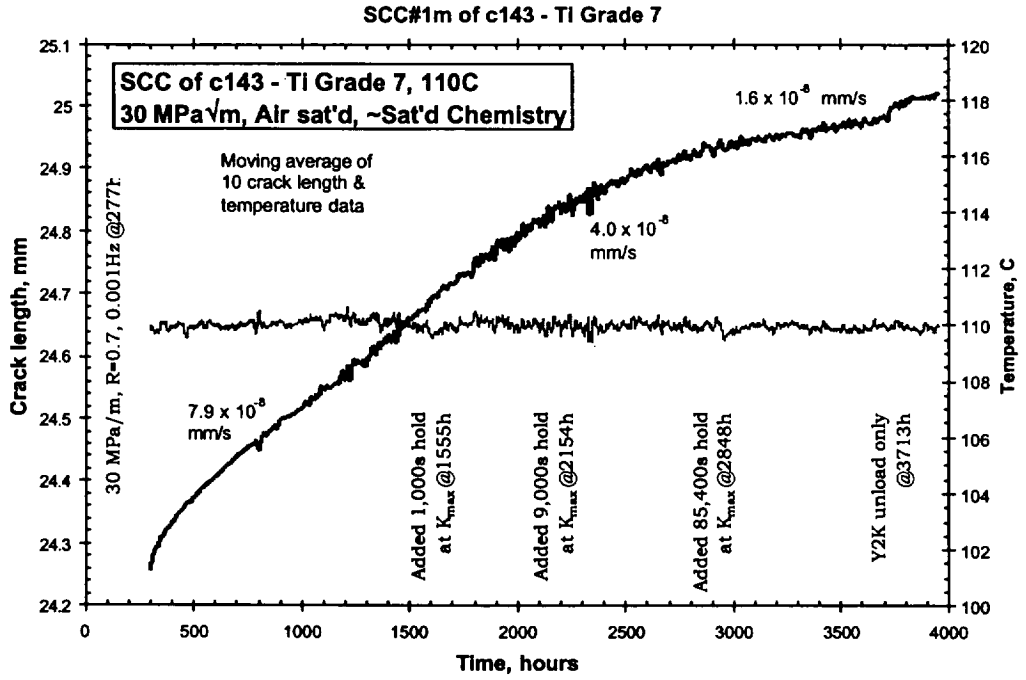

Figure 1. Crack length and temperature vs. time plot of the stress corrosion cracking response of specimen c143 (as-received Titanium Grade 7) at 110 °C in a concentrated mixed salt environment with 5 psi over-pressure of laboratory air.

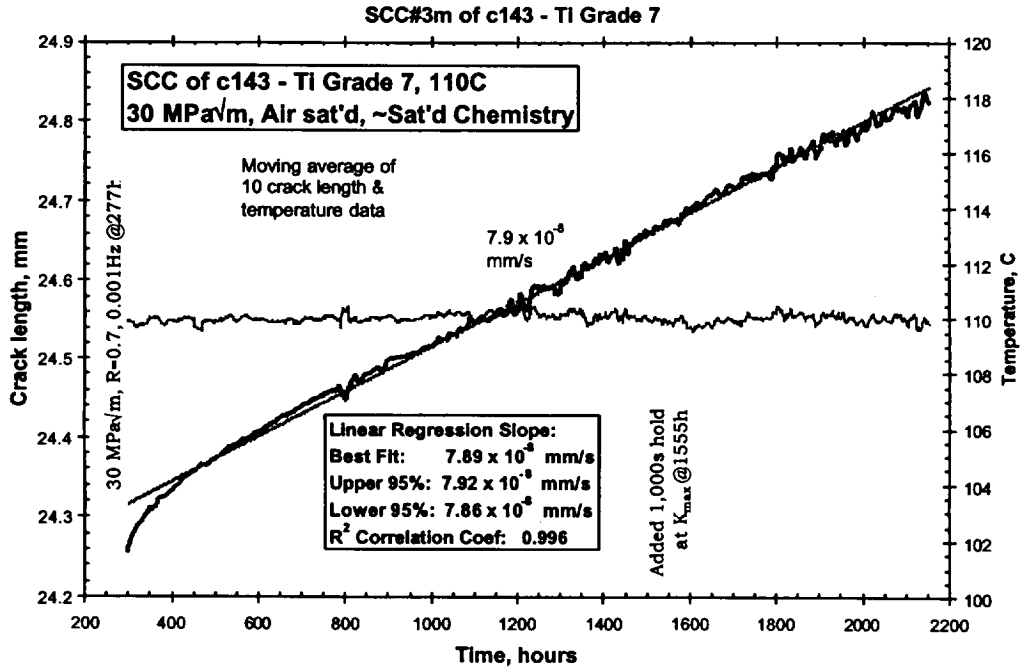

Figure 2. Crack length and temperature vs. time plot of the stress corrosion cracking response of specimen c143 (as-received Titanium Grade 7) at 110 °C in a concentrated mixed salt environment with 5 psi over-pressure of laboratory air.

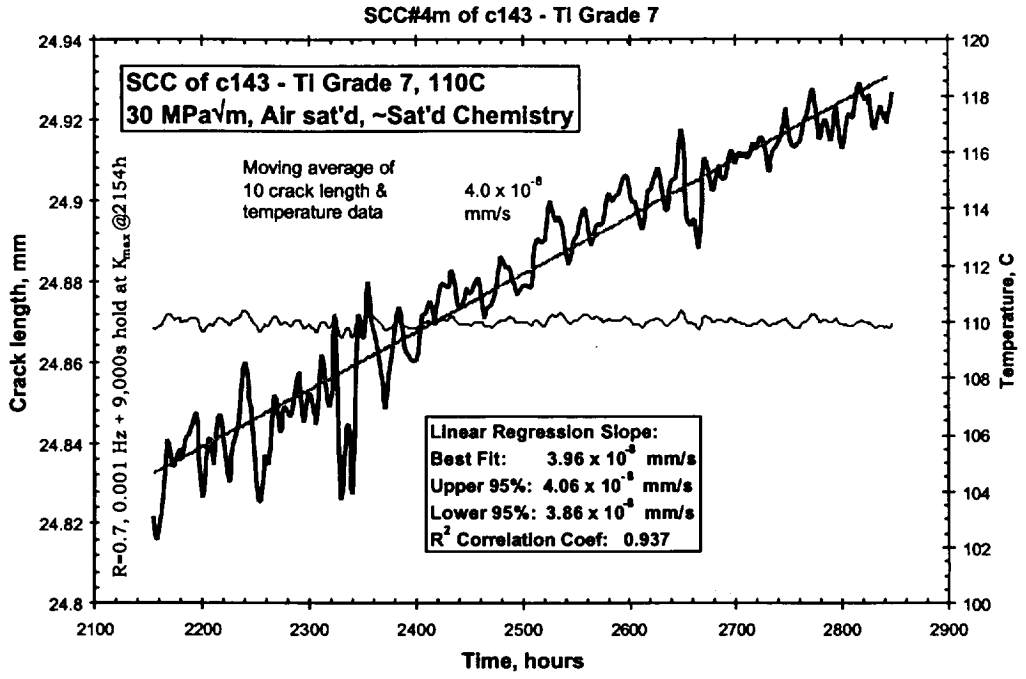

Figure 3. Crack length and temperature vs. time plot of the stress corrosion cracking response of specimen c143 (as-received Titanium Grade 7) at 110 °C in a concentrated mixed salt environment with 5 psi over-pressure of laboratory air.

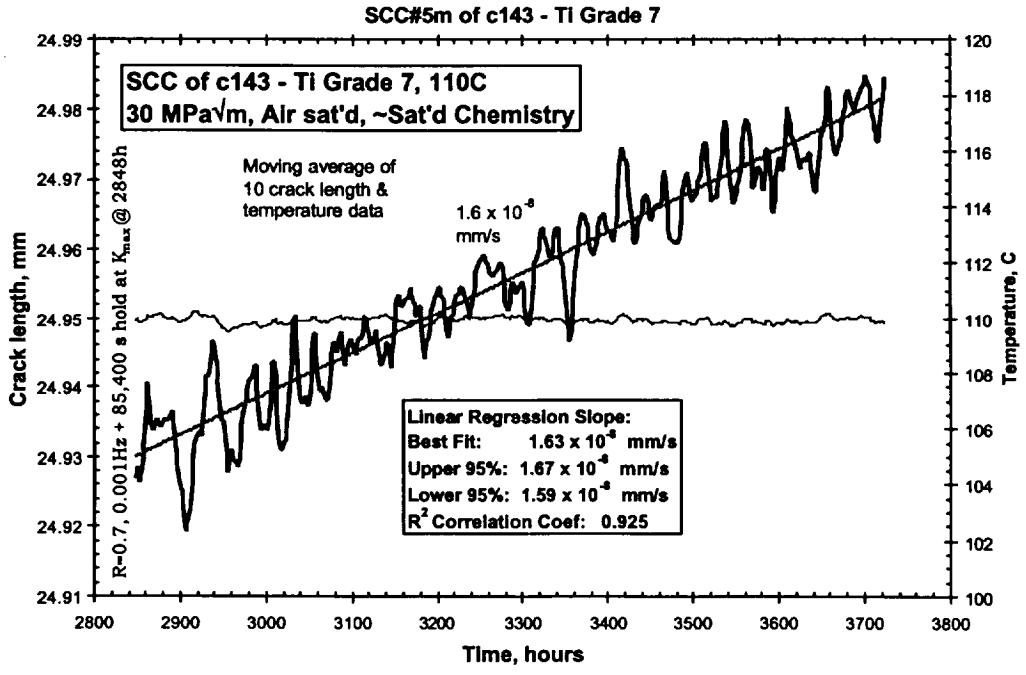

Figure 4. Crack length and temperature vs. time plot of the stress corrosion cracking response of specimen c143 (as-received Titanium Grade 7) at 110 °C in a concentrated mixed salt environment with 5 psi over-pressure of laboratory air.

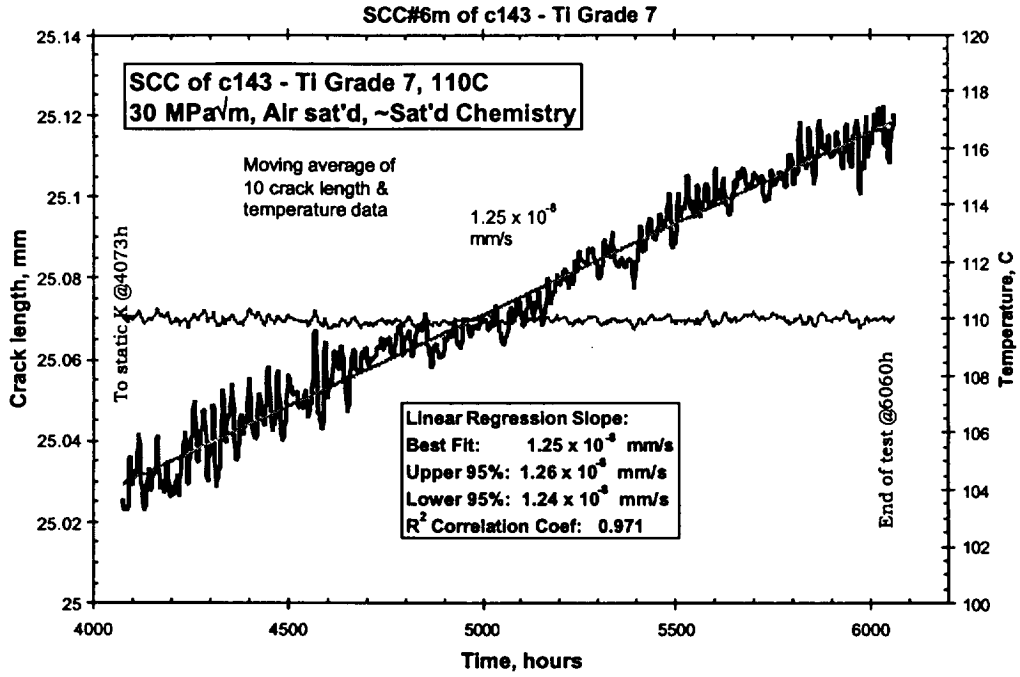

Figure 5. Crack length and temperature vs. time plot of the stress corrosion cracking response of specimen c143 (as-received Titanium Grade 7) at 110 °C in a concentrated mixed salt environment with 5 psi over-pressure of laboratory air.

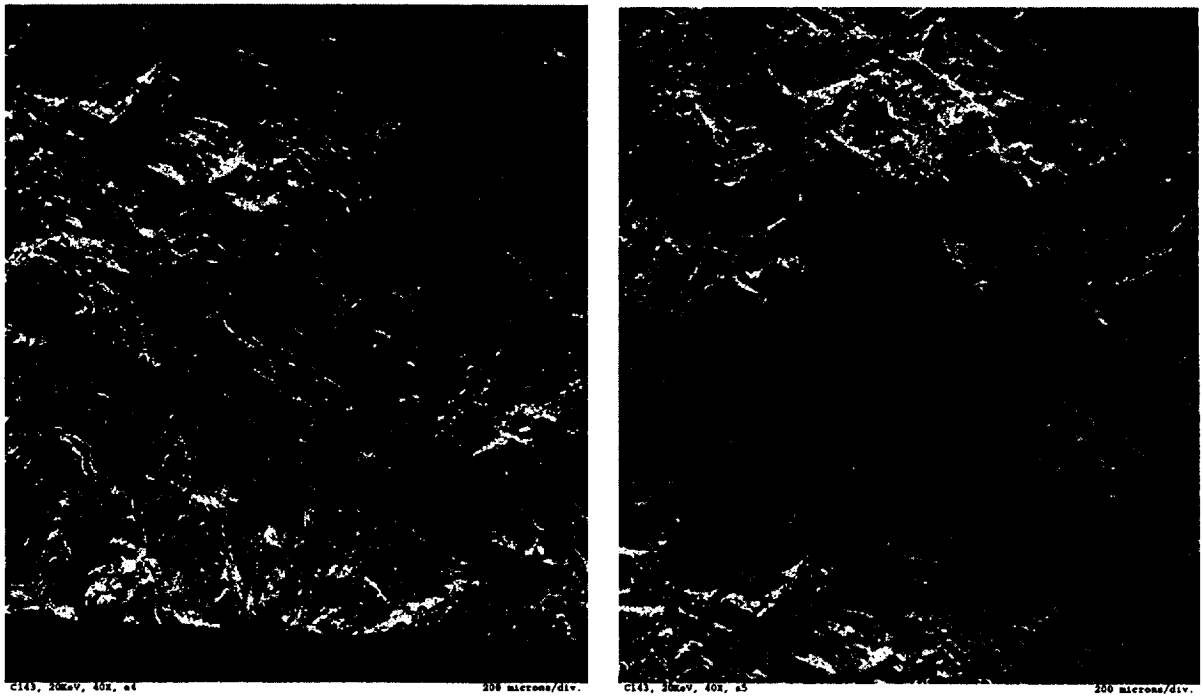

Figure 6. Scanning electron microscopic examination of specimen c143 (as-received Titanium Grade 7) after testing at 110 °C in a concentrated mixed salt environment with 5 psi over-pressure of laboratory air. The micrograph on the right is a "continuation" of the top of the one on the left. The cracking morphology is completely transgranular – no evidence of intergranular cracking was observed.

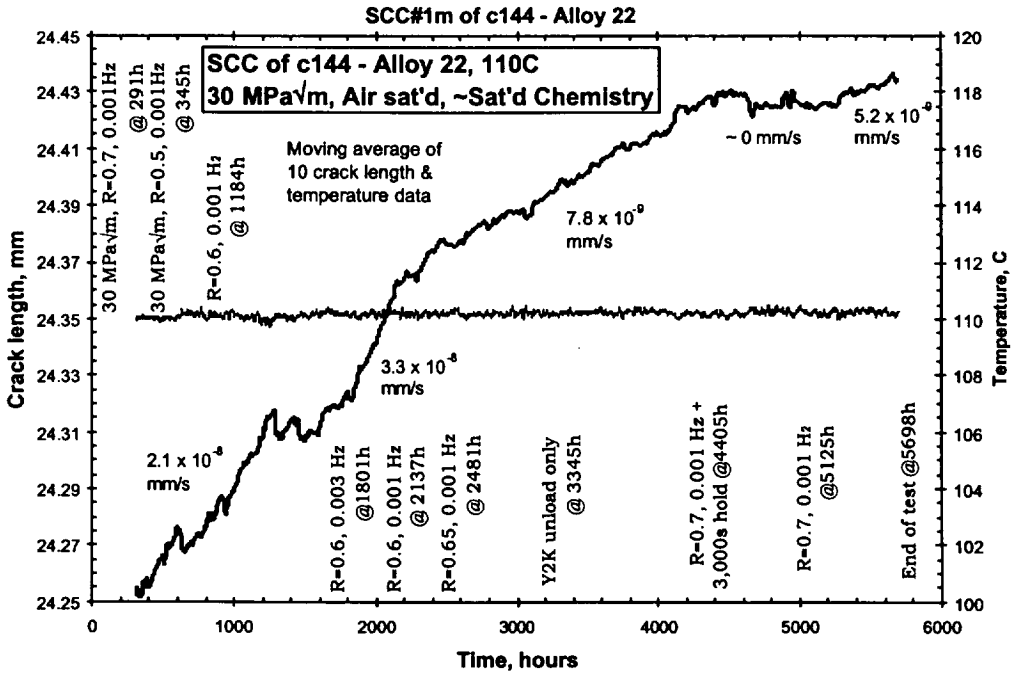

Figure 7. Crack length and temperature vs. time plot of the stress corrosion cracking response of specimen c144 (as-received Alloy C-22 base metal) at 110 °C in a concentrated mixed salt environment with 5 psi over-pressure of laboratory air.

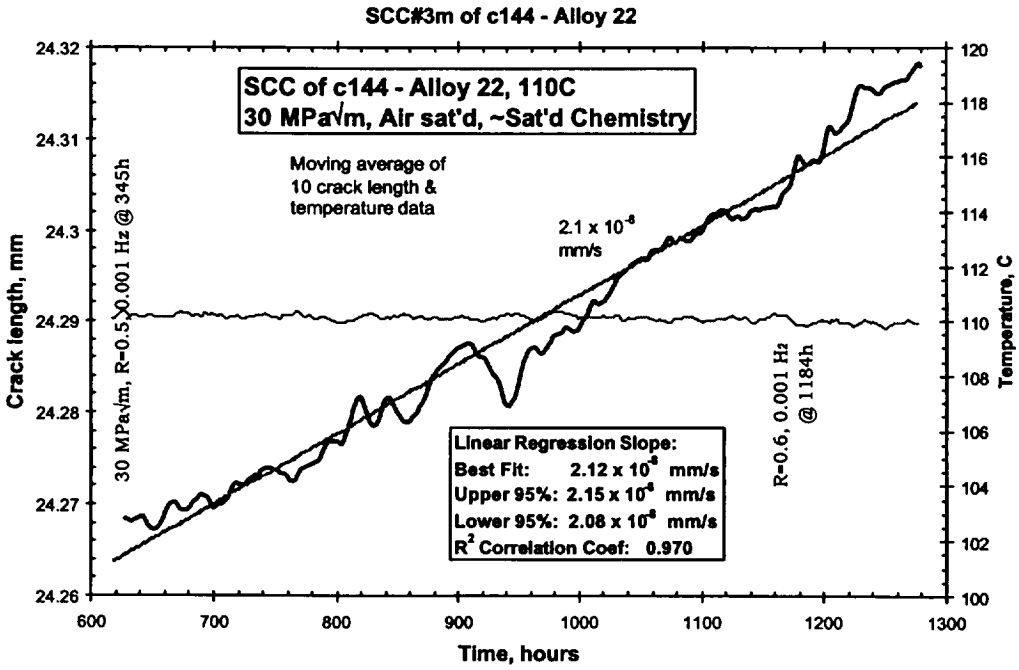

Figure 8. Crack length and temperature vs. time plot of the stress corrosion cracking response of specimen c144 (as-received Alloy C-22 base metal) at 110 °C in a concentrated mixed salt environment with 5 psi over-pressure of laboratory air.

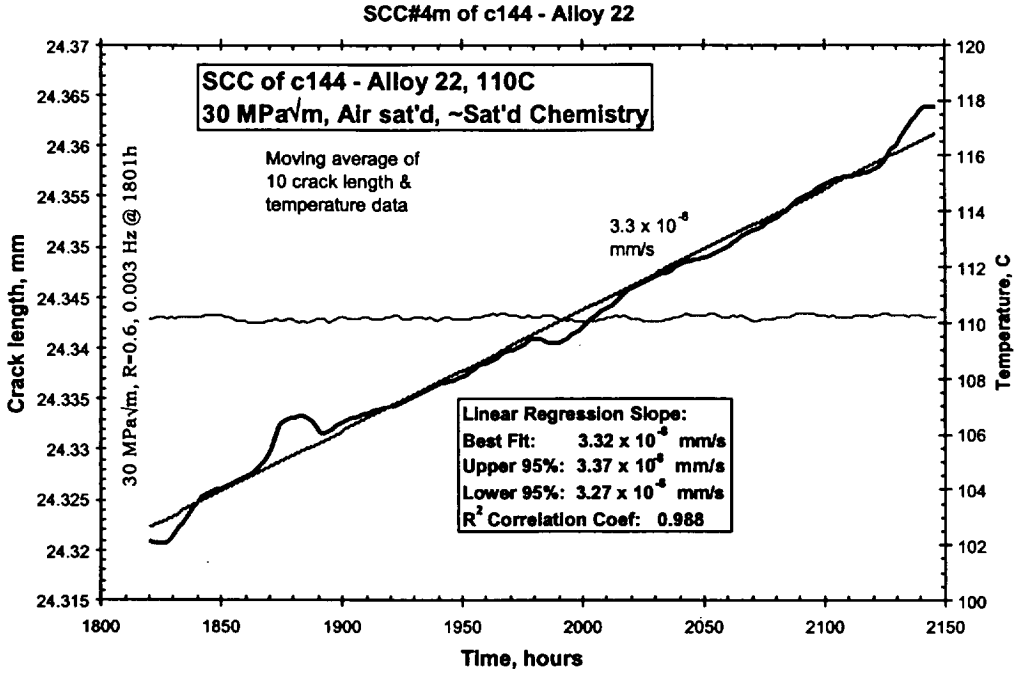

Figure 9. Crack length and temperature vs. time plot of the stress corrosion cracking response of specimen c144 (as-received Alloy C-22 base metal) at 110 °C in a concentrated mixed salt environment with 5 psi over-pressure of laboratory air.

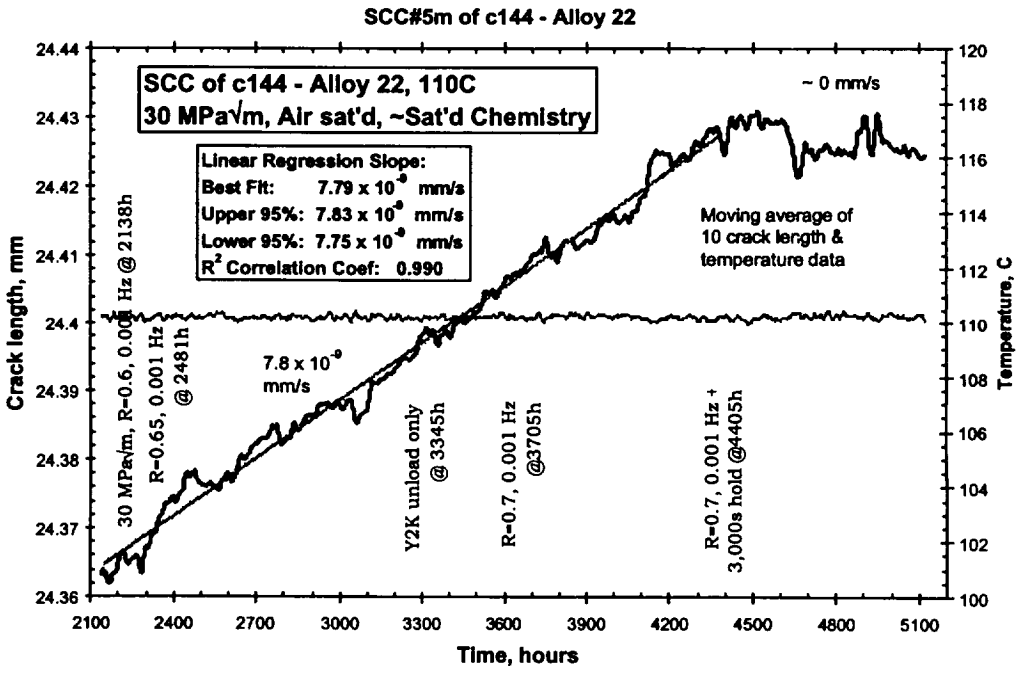

Figure 10. Crack length and temperature vs. time plot of the stress corrosion cracking response of specimen c144 (as-received Alloy C-22 base metal) at 110 °C in a concentrated mixed salt environment with 5 psi over-pressure of laboratory air.

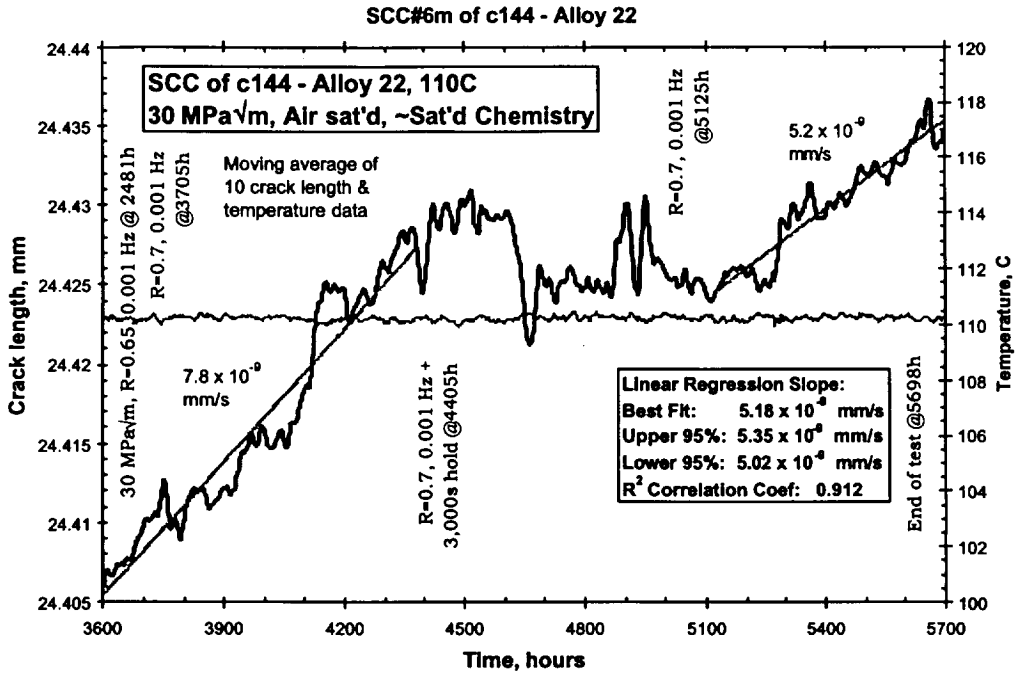

Figure 11. Crack length and temperature vs. time plot of the stress corrosion cracking response of specimen c144 (as-received Alloy C-22 base metal) at 110 °C in a concentrated mixed salt environment with 5 psi over-pressure of laboratory air.

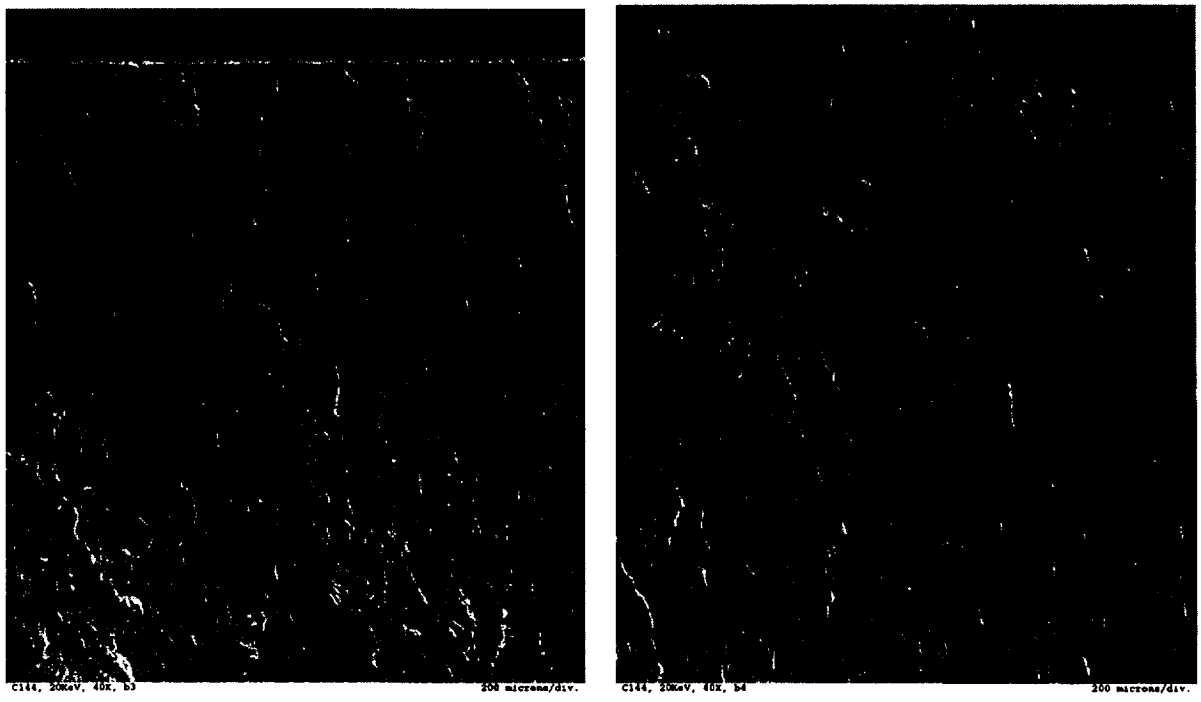

Figure 12. Scanning electron microscopic examination of specimen c144 (as-received Alloy 22) after testing at 110 °C in a concentrated mixed salt environment with 5 psi over-pressure of laboratory air. The image on the right overlaps with the bottom of the image on the left. The cracking morphology is completely transgranular – no evidence of intergranular cracking was observed.

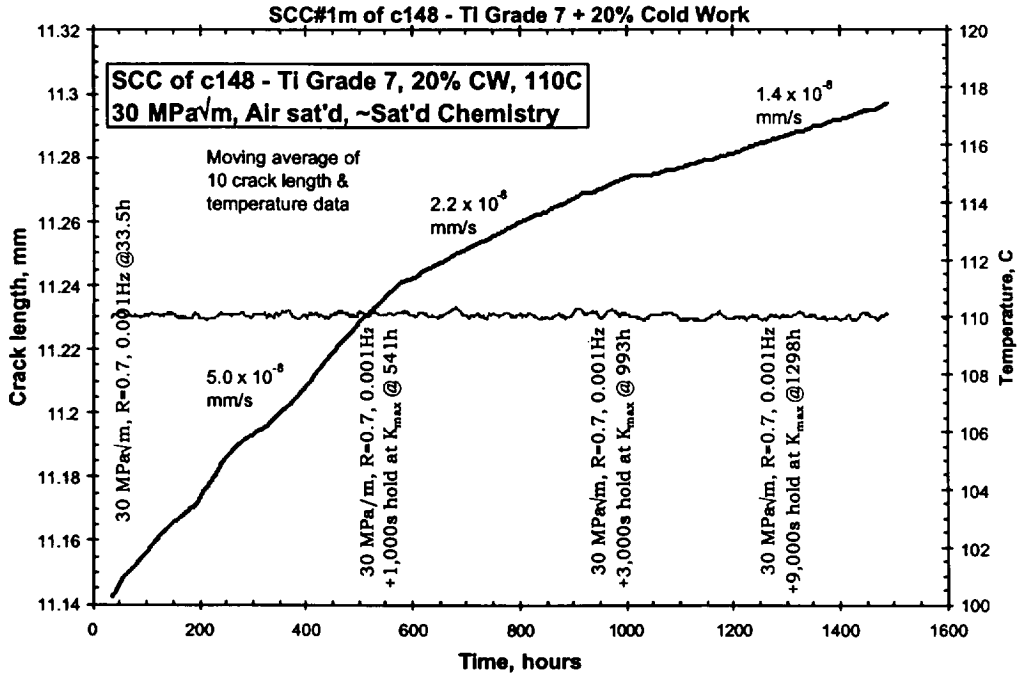

Figure 13. Crack length and temperature vs. time plot of the stress corrosion cracking response of specimen c148 (a 0.5TCT of 20% cold worked Titanium Grade 7) at 110 °C in a concentrated mixed salt environment with 5 psi over-pressure of laboratory air.

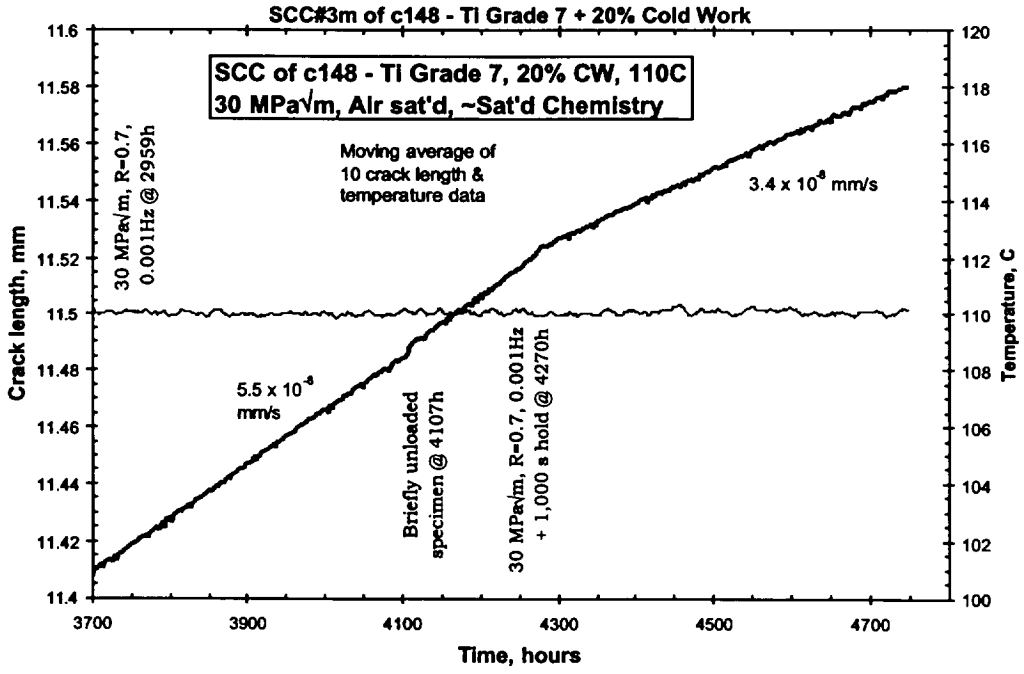

Figure 14. Crack length and temperature vs. time plot of the stress corrosion cracking response of specimen c148 (a 0.5TCT of 20% cold worked Titanium Grade 7) at 110 °C in a concentrated mixed salt environment with 5 psi over-pressure of laboratory air.

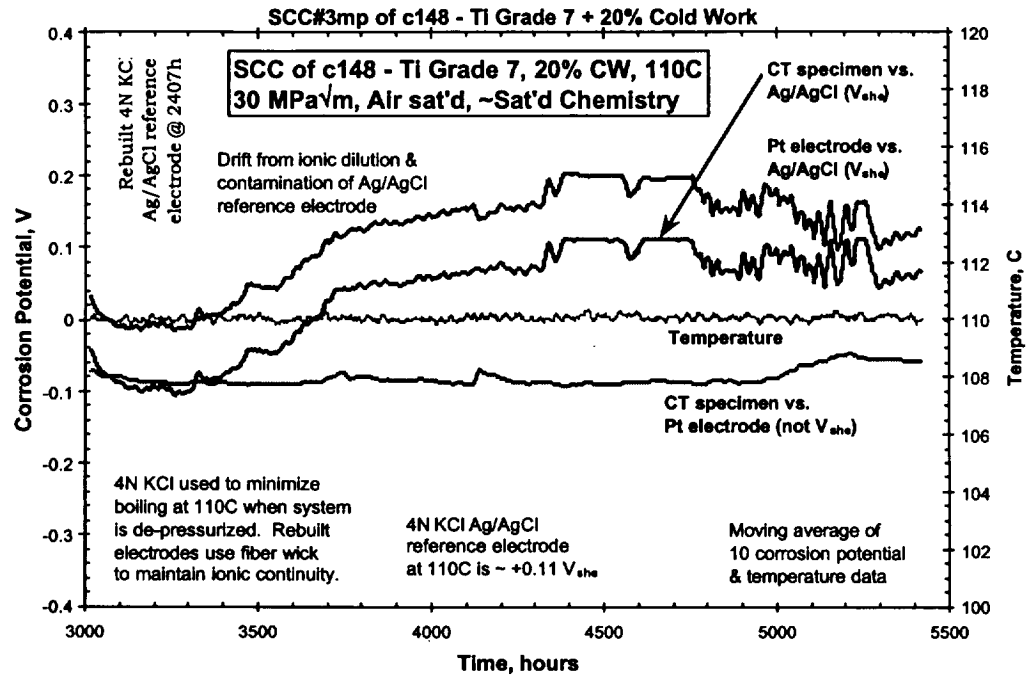

Figure 15. Corrosion potential vs. time plot of the corrosion potential response of specimen c148 (a 0.5TCT of 20% cold worked Titanium Grade 7) at 110 °C in a concentrated mixed salt environment with 5 psi over-pressure of laboratory air.

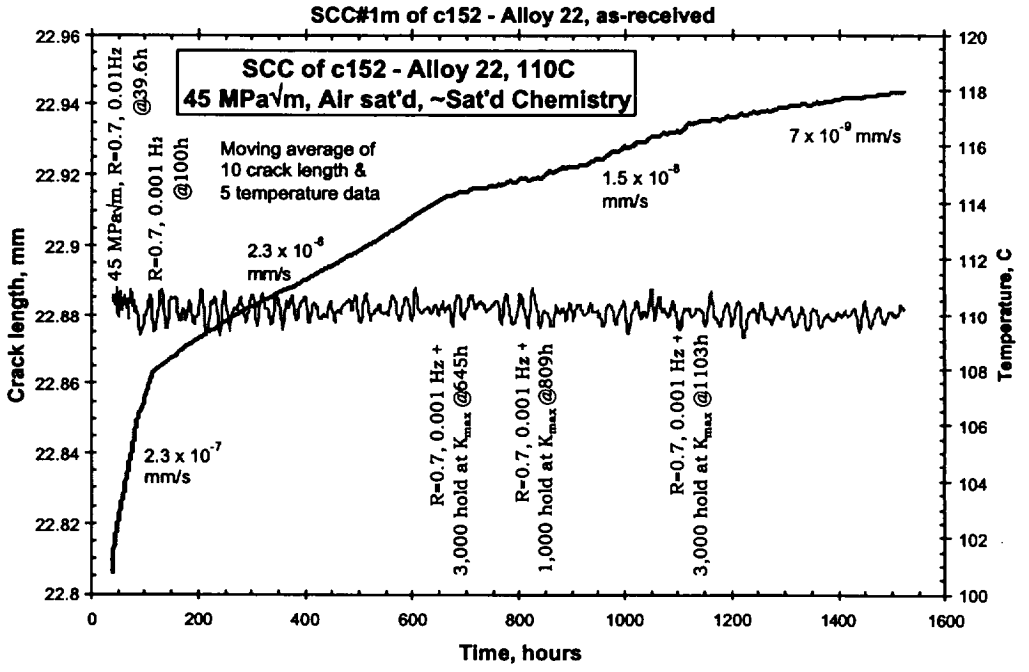

Figure 16. Crack length and temperature vs. time plot of the stress corrosion cracking response of specimen c152 (a 1TCT of as-received Alloy 22) at 110 °C in a concentrated mixed salt environment with 5 psi over-pressure of laboratory air.

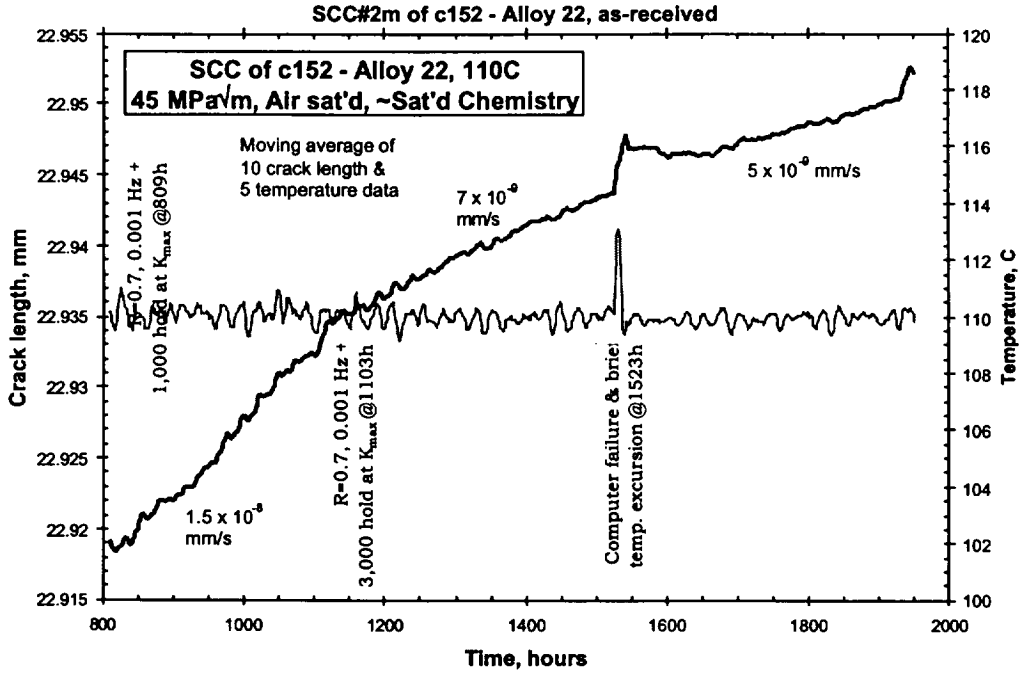

Figure 17. Crack length and temperature vs. time plot of the stress corrosion cracking response of specimen c152 (a 1TCT of as-received Alloy 22) at 110 °C in a concentrated mixed salt environment with 5 psi over-pressure of laboratory air.

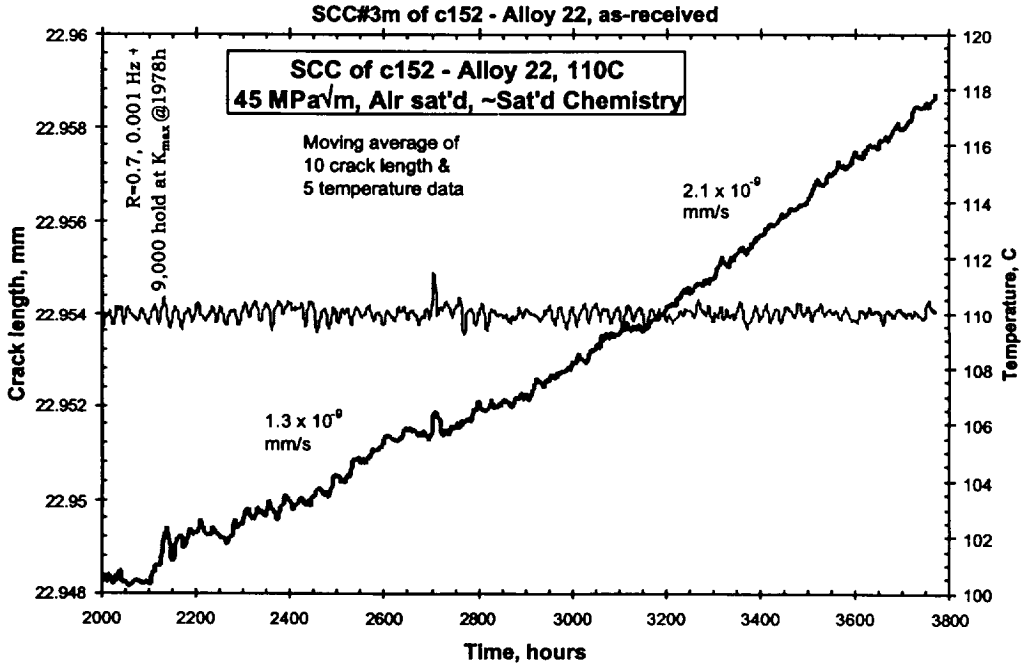

Figure 18. Crack length and temperature vs. time plot of the stress corrosion cracking response of specimen c152 (a 1TCT of as-received Alloy 22) at 110 °C in a concentrated mixed salt environment with 5 psi over-pressure of laboratory air.

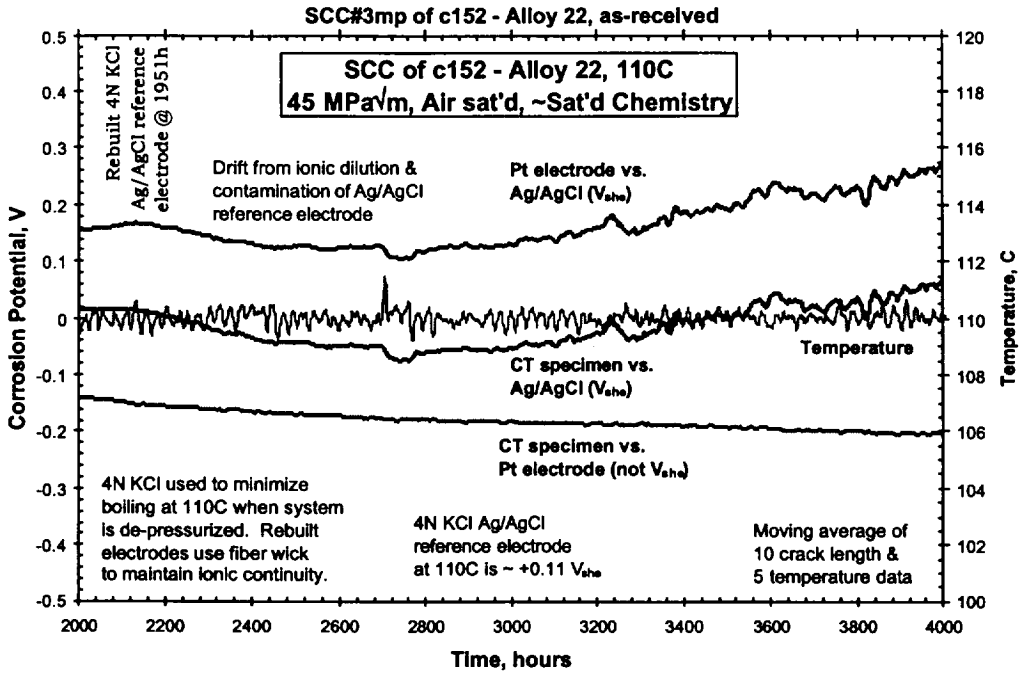

Figure 19. Corrosion potential vs. time plot of the corrosion potential response of specimen c152 (a 1TCT of as-received Alloy 22) at 110 °C in a concentrated mixed salt environment with 5 psi over-pressure of laboratory air.

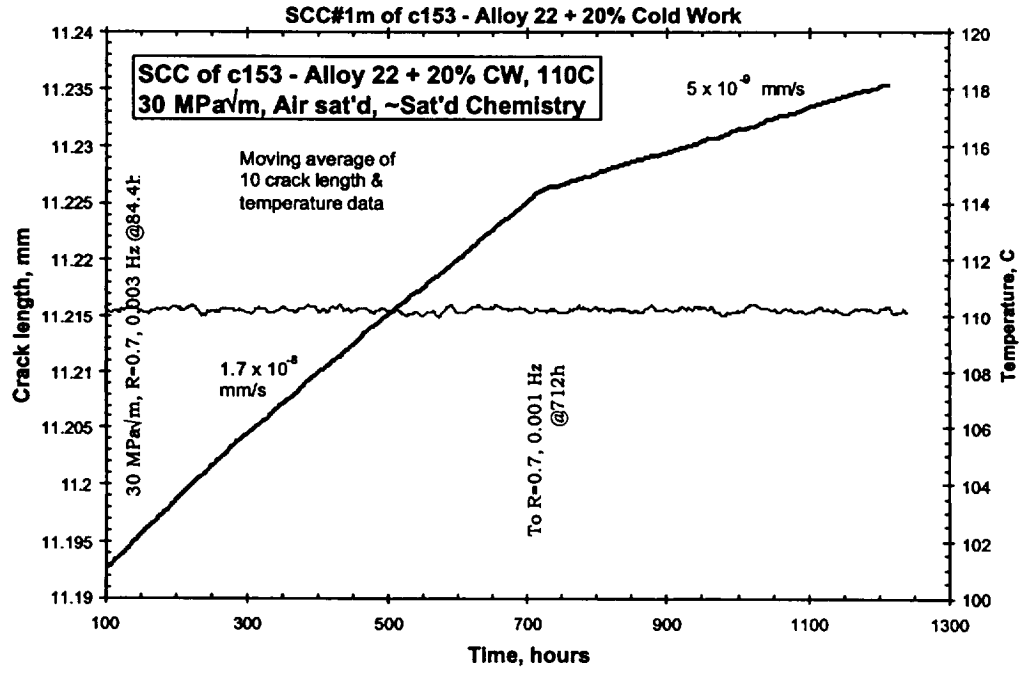

Figure 20. Crack length and temperature vs. time plot of the stress corrosion cracking response of specimen c153 (a 0.5TCT of 20% cold worked Alloy 22) at 110 °C in a concentrated mixed salt environment with 5 psi over-pressure of laboratory air.

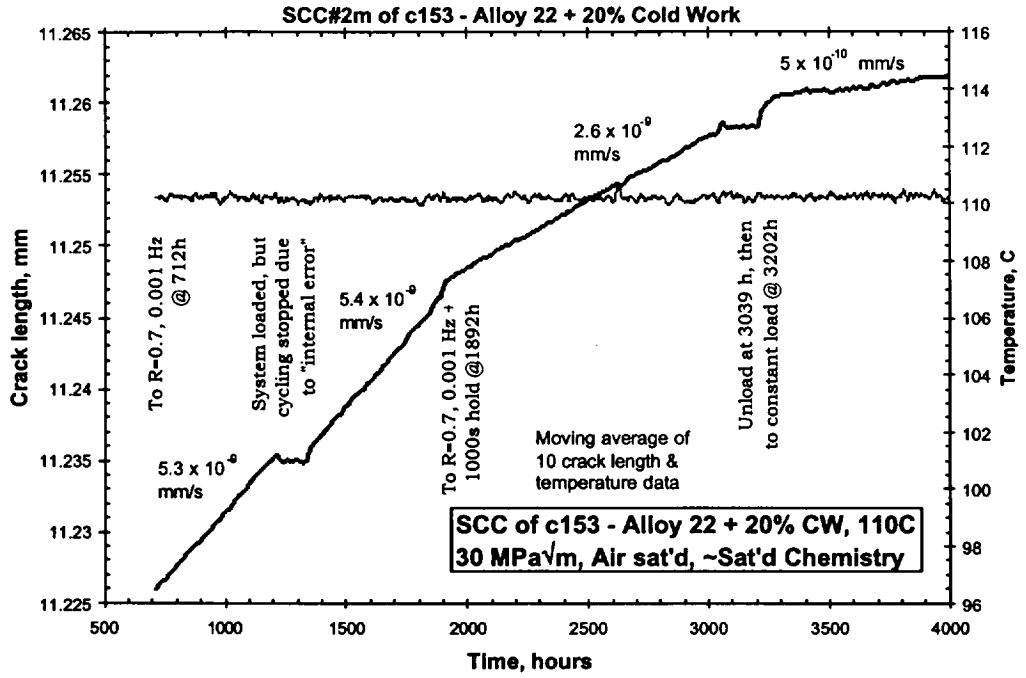

Figure 21. Crack length and temperature vs. time plot of the stress corrosion cracking response of specimen c153 (a 0.5TCT of 20% cold worked Alloy 22) at 110 °C in a concentrated mixed salt environment with 5 psi over-pressure of laboratory air.

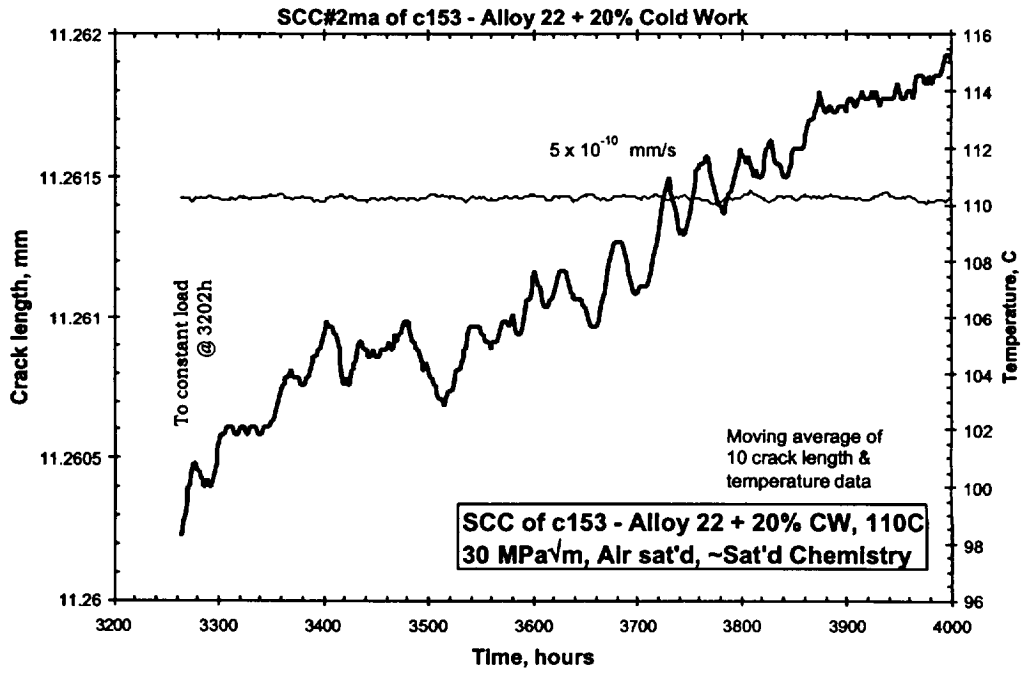

Figure 22. Crack length and temperature vs. time plot of the stress corrosion cracking response of specimen c153 (a 0.5TCT of 20% cold worked Alloy 22) at 110 °C in a concentrated mixed salt environment with 5 psi over-pressure of laboratory air.

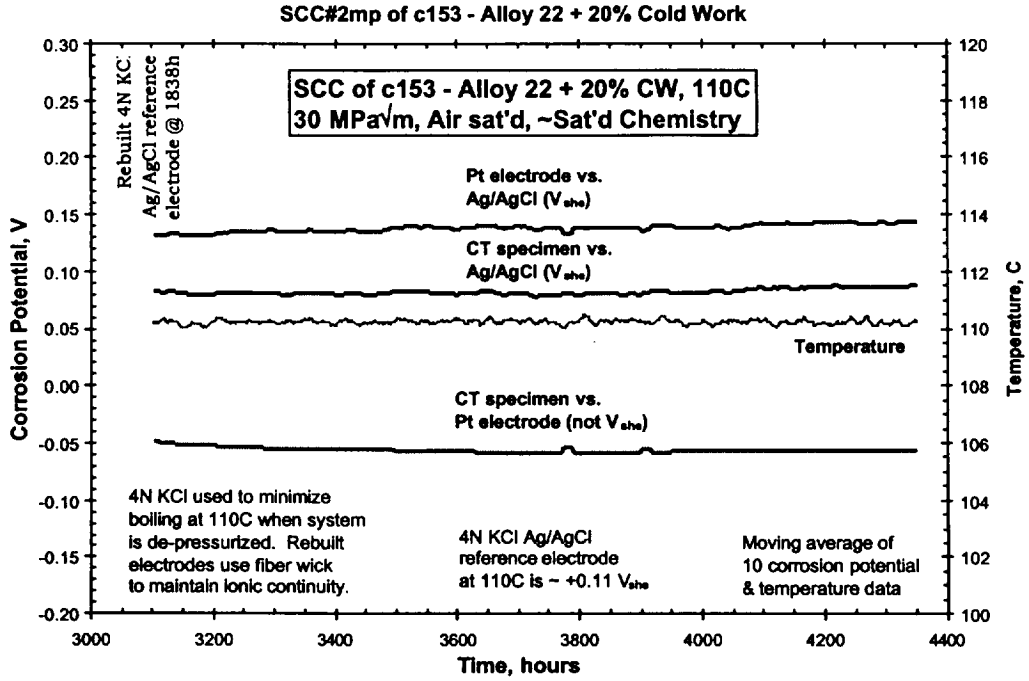

Figure 23. Corrosion potential vs. time plot of the corrosion potential response of specimen c153 (a 0.5TCT of 20% cold worked Alloy 22) at 110 °C in a concentrated mixed salt environment with 5 psi over-pressure of laboratory air.

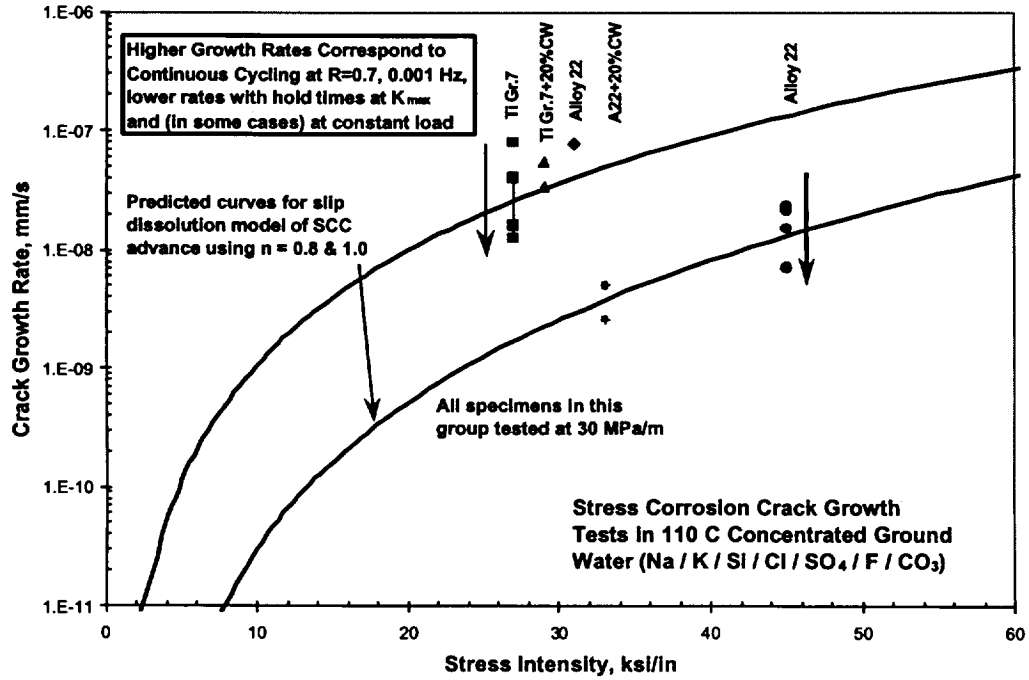

Figure 24. Comparison of results with predicted behavior based on stress corrosion crack growth rate modeling developed for stainless steels in 288 °C water – the predictions are based on unaggressive conditions (fast repassivation), which is consistent with the nature of the alloys tested and mixed ions / high pH environment.

LIST OF FIGURES

Figure 7. Crack length and temperature vs. time plot of the stress corrosion cracking response of specimen c144 (as-received Alloy C-22 base metal) at 110 °C in a concentrated mixed salt environment with 5 psi over-pressure of laboratory air.

Figure 8. Crack length and temperature vs. time plot of the stress corrosion cracking response of specimen c144 (as-received Alloy C-22 base metal) at 110 °C in a concentrated mixed salt environment with 5 psi over-pressure of laboratory air.

Figure 9. Crack length and temperature vs. time plot of the stress corrosion cracking response of specimen c144 (as-received Alloy C-22 base metal) at 110 °C in a concentrated mixed salt environment with 5 psi over-pressure of laboratory air.

Figure 10. Crack length and temperature vs. time plot of the stress corrosion cracking response of specimen c144 (as-received Alloy C-22 base metal) at 110 °C in a concentrated mixed salt environment with 5 psi over-pressure of laboratory air.

Figure 11. Crack length and temperature vs. time plot of the stress corrosion cracking response of specimen c144 (as-received Alloy C-22 base metal) at 110 °C in a concentrated mixed salt environment with 5 psi over-pressure of laboratory air.

Figure 12. Scanning electron microscopic examination of specimen c144 (as-received Alloy 22) after testing at 110 °C in a concentrated mixed salt environment with 5 psi over-pressure of laboratory air. The image on the right overlaps with the bottom of the image on the left. The cracking morphology is completely transgranular – no evidence of intergranular cracking was observed.

Figure 13. Crack length and temperature vs. time plot of the stress corrosion cracking response of specimen c148 (a 0.5TCT of 20% cold worked Titanium Grade 7) at 110 °C in a concentrated mixed salt environment with 5 psi over-pressure of laboratory air.

Figure 14. Crack length and temperature vs. time plot of the stress corrosion cracking response of specimen c148 (a 0.5TCT of 20% cold worked Titanium Grade 7) at 110 °C in a concentrated mixed salt environment with 5 psi over-pressure of laboratory air.

Figure 15. Corrosion potential vs. time plot of the corrosion potential response of specimen c148 (a 0.5TCT of 20% cold worked Titanium Grade 7) at 110 °C in a concentrated mixed salt environment with 5 psi over-pressure of laboratory air.

Figure 16. Crack length and temperature vs. time plot of the stress corrosion cracking response of specimen c152 (a 1TCT of as-received Alloy 22) at 110 °C in a concentrated mixed salt environment with 5 psi over-pressure of laboratory air.

Figure 17. Crack length and temperature vs. time plot of the stress corrosion cracking response of specimen c152 (a 1TCT of as-received Alloy 22) at 110 °C in a concentrated mixed salt environment with 5 psi over-pressure of laboratory air.

Figure 18. Crack length and temperature vs. time plot of the stress corrosion cracking response of specimen c152 (a 1TCT of as-received Alloy 22) at 110 °C in a concentrated mixed salt environment with 5 psi over-pressure of laboratory air.

Figure 19. Corrosion potential vs. time plot of the corrosion potential response of specimen c152 (a 1TCT of as-received Alloy 22) at 110 °C in a concentrated mixed salt environment with 5 psi over-pressure of laboratory air.

Figure 20. Crack length and temperature vs. time plot of the stress corrosion cracking response of specimen c153 (a 0.5TCT of 20% cold worked Alloy 22) at 110 °C in a concentrated mixed salt environment with 5 psi over-pressure of laboratory air.

Figure 21. Crack length and temperature vs. time plot of the stress corrosion cracking response of specimen c153 (a 0.5TCT of 20% cold worked Alloy 22) at 110 °C in a concentrated mixed salt environment with 5 psi over-pressure of laboratory air.

Figure 22. Crack length and temperature vs. time plot of the stress corrosion cracking response of specimen c153 (a 0.5TCT of 20% cold worked Alloy 22) at 110 °C in a concentrated mixed salt environment with 5 psi over-pressure of laboratory air.

Figure 23. Corrosion potential vs. time plot of the corrosion potential response of specimen c153 (a 0.5TCT of 20% cold worked Alloy 22) at 110 °C in a concentrated mixed salt environment with 5 psi over-pressure of laboratory air.

Figure 24. Comparison of results with predicted behavior based on stress corrosion crack growth rate modeling developed for stainless steels in 288 °C water – the predictions are based on unaggressive conditions (fast repassivation), which is consistent with the nature of the alloys tested and mixed ions / high pH environment.